DOI: 10.1002/ejic.200900336

Rare-Earth Tetrel Antimonides $RE_5Tt_xSb_{3-x}$ (RE = La–Nd; Tt = Si, Ge)

Haiying Bie[a] and Arthur Mar*[a]

Keywords: Rare earths / Group 14 elements / Antimony / Intermetallic phases / Magnetic properties

Ternary rare-earth tetrel antimonides $RE_5Tt_xSb_{3-x}$ (RE = La–Nd; Tt = Si, Ge) have been prepared by arc-melting of the elements and annealing at 800 °C. Their crystal structures were determined by single-crystal and powder X-ray diffraction methods. These ternary antimonides adopt a structure (β-Yb_5Sb_3-type, orthorhombic, space group $Pnma$, $Z = 4$) that is different from those of the parent binary phases RE_5Sb_3 (Mn_5Si_3-type), RE_5Si_3 (Cr_5B_3-type), or RE_5Ge_3 (Mn_5Si_3-type) for RE = La–Nd. The range of solid solubility determined for a representative series, $La_5Ge_xSb_{3-x}$, is relatively wide, $0.9 \leq x \leq 1.6$. The disorder arises largely from the partial substitution of Tt atoms into Sb sites centred within RE_6 trigonal prisms. Columns of confacial RE_6 trigonal prisms are connected to each other through edge-sharing to form a three-dimensional framework outlining hexagonal channels filled by ribbons of $[RE_2Tt_2]$ rhombs. Band-structure calculations provided support for these site preferences and the range of solid solubility in $La_5Ge_xSb_{3-x}$, which can be related largely to changes in the heteroatomic La–Ge and La–Sb bonding interactions. Magnetic measurements on $RE_5Tt_xSb_{3-x}$ (RE = La, Pr, Nd) revealed Pauli paramagnetic behaviour for the La members and multiple low-temperature transitions (likely involving ferromagnetic ordering) for the Pr and Nd members.

(© Wiley-VCH Verlag GmbH & Co. KGaA, 69451 Weinheim, Germany, 2009)

Introduction

In giant magnetocaloric materials such as the intermetallic compounds based on Gd_5Ge_4, a ferromagnetic ordering should be accompanied by a structural phase transition.[1] These structural changes can be induced not only by controlling physical variables such as temperature or magnetic field, but also by manipulating the chemical composition through varying the valence-electron concentration (e.g., $Gd_5Ga_xGe_{4-x}$),[2] cation or anion size (e.g., $Gd_{5-x}Y_xGe_4$, $Gd_5Si_xGe_{4-x}$),[3,4] or both (e.g., $La_{5-x}Ca_xGe_4$, $Gd_5Sb_xGe_{4-x}$).[5,6] Recently, efforts have been made to prepare ternary derivatives based on another class of intermetallic compounds, the binary rare-earth antimonides RE_5Sb_3, as potential magnetocaloric materials.[7] The binary RE_5Sb_3 phases adopt different crystal structures depending on the RE.[8] The hexagonal Mn_5Si_3-type structure predominates for most of the RE elements, but the orthorhombic β-Yb_5Sb_3-type and Y_5Bi_3-type structures are also found less commonly, usually for the later RE elements.[9] (Although it is now recognized that the eponymous "β-Yb_5Sb_3" does not exist as a true binary but rather as a hydrogen-stabilized phase,[10,11] the name of this structure type has conventionally been retained to describe other genuine binary phases.) Interestingly, chemical substitution of the Sb atoms in RE_5Sb_3 results in nonstoichiometric $RE_5M_xSb_{3-x}$ (RE = Gd–Er, Y; M = Fe, Co, Ni, Cu; $x \leq 1$) phases that adopt the β-Yb_5Sb_3-type structure.[7,12–15] So far, the substitution has been limited to transition metals for M, whereas substitution by p-block elements has not been attempted.

Here, we report the existence of new $RE_5Tt_xSb_{3-x}$ series containing an early rare-earth (RE = La–Nd) and a p-block element from group 14 (a tetrel, Tt = Si, Ge). This substitution, which changes both the electron count and anion size, stabilizes the formation of the orthorhombic β-Yb_5Sb_3-type structure, different from those of the parent binaries (RE_5Sb_3, RE_5Si_3, or RE_5Ge_3). Band-structure calculations were carried out to gain further understanding of the factors influencing the structure and bonding of these compounds. As initial steps to characterize their materials properties, magnetic measurements were also made.

Results and Discussion

Phase Relationships

Because limited information was previously available about phase relationships in the RE–Si–Sb systems (whose phase diagrams have been determined only for RE = Ce, Dy, and Y),[16–18] initial investigations were carried out to elaborate the La–Si–Sb phase diagram. Through powder X-ray diffraction and energy-dispersive X-ray analysis on 37 arc-melted samples, the isothermal section at 800 °C was constructed (Figure 1). The existence of expected binary La–Si and La–Sb phases and the absence of binary Si–Sb phases were confirmed.[19] In the La–Si system, two Si-rich

[a] Department of Chemistry, University of Alberta, Edmonton, AB T6G 2G2, Canada
Fax: +1-780-492-8231
E-mail: arthur.mar@ualberta.ca

Supporting information for this article is available on the WWW under http://dx.doi.org/10.1002/ejic.200900336.

 © 2009 Wiley-VCH Verlag GmbH & Co. KGaA, Weinheim

phases exhibited slight homogeneity ranges. In $LaSi_2$ ($ThSi_2$-type, space group $I4_1/amd$), a deficiency of up to 10% Si was observed. In $LaSi_{2-x}$ ($GdSi_{1.4}$-type, space group *Imma*), a homogeneity range of $0.3 \leq x \leq 0.5$ was found. Of the two modifications known for LaSi, only the high-temperature form (FeB-b-type, space group *Pnma*) was formed. La_5Si_3 also adopts two possible modifications, but only the tetragonal form (Cr_5B_3-type, space group $I4/mcm$) was observed. In the La–Sb system, the phases formed at 800 °C are consistent with previously reported phase diagrams, for the most part, except that La_5Sb_3 and La_4Sb_3 should replace the non-existent "La_3Sb_2" phase.[19] These observations on La–Sb phases agree with our recent investigation of the La–Ti–Sb phase diagram.[20]

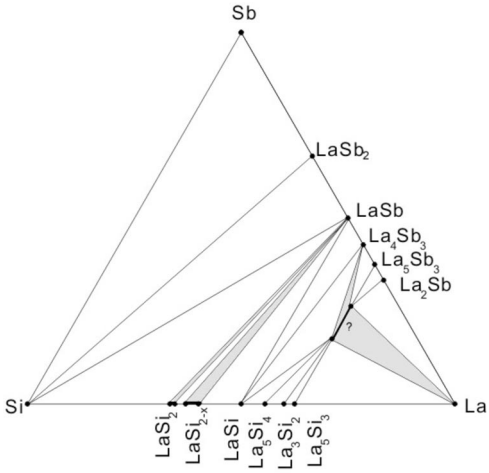

Figure 1. Isothermal section at 800 °C for the La–Si–Sb system. The ternary phase is identified to be $La_5Si_xSb_{3-x}$, with a homogeneity width estimated to be similar to that in $La_5Ge_xSb_{3-x}$ ($0.9 \leq x \leq 1.6$).

A new ternary phase $La_5Si_xSb_{3-x}$ was identified in the vicinity of the composition La/Si/Sb = 65:15:20 in the La–Si–Sb phase diagram. The germanium-containing analogue $La_5Ge_xSb_{3-x}$ was also identified in the La–Ge–Sb phase diagram, which is more complicated and whose investigation is still in progress.[21] Because La_5Sb_3 and La_5Ge_3 are isostructural, both adopting the hexagonal Mn_5Si_3-type structure, the initial thought was that the ternary phase represented a solid solution of the component binary phases. However, analysis of the products obtained from arc-melting reactions with various loading compositions $La_5Ge_xSb_{3-x}$ ($0 \leq x \leq 3$) revealed that the solid solubility extends only within the range $0.9 \leq x \leq 1.6$ (Figure 2; Table S1), and that the structure is of the orthorhombic β-Yb_5Sb_3-type, different from those of the parent binaries RE_5Sb_3 (Mn_5Si_3-type), RE_5Si_3 (Cr_5B_3-type), or RE_5Ge_3 (Mn_5Si_3-type) for *RE* = La–Nd.

These ternary phases represent the first examples of cases where the β-Yb_5Sb_3-type structure can be stabilized by replacement of Sb with another *p*-block element instead of a transition metal, as was previously known.[7,12–15] Interestingly, attempts to synthesize the analogous ternary $RE_5Tt_xSb_{3-x}$ (*Tt* = Si, Ge) phases with other rare-earth

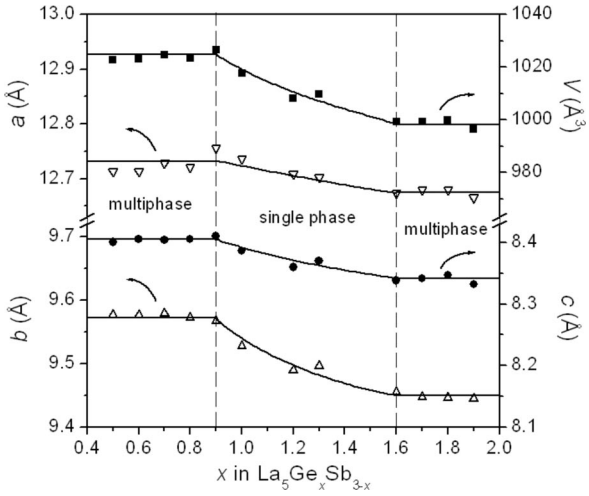

Figure 2. Plot of cell parameters vs. x for the β-Yb_5Sb_3-type phase obtained in reactions with nominal composition $La_5Ge_xSb_{3-x}$. In addition to the ternary phase, La_5Sb_3 and La_4Sb_3 were also formed below x = 0.9, and La_4Ge_3 was formed above x = 1.6.

metals indicated that the range of substitution is limited to the earlier or larger members (*RE* = La–Nd), in contrast to the $RE_5M_xSb_{3-x}$ (*M* = Fe, Co, Ni, Cu) phases which are stabilized in the presence of the later or smaller members (*RE* = Gd–Er, Y). Examples of compounds characterized in this study by X-ray diffraction and elemental analysis are listed in Table 1.

Table 1. Atomic compositions [%] determined from X-ray diffraction data and electron probe microanalysis data for $RE_5Tt_xSb_{3-x}$ (*RE* = La–Nd; *Tt* = Si, Ge).

Formula from X-ray data	Expected			Observed		
	RE	*Tt*	Sb	*RE*	*Tt*	Sb
$La_5Si_{1.40(2)}Sb_{1.60(2)}$	62.5	17.5	20.0	not measured		
$Ce_5Si_{1.4}Sb_{1.6}$[a]	62.5	17.5	20.0	62.4(4)	18.2(6)	19.3(4)
$Pr_5Si_{1.20(3)}Sb_{1.800(8)}$	62.5	15.0	22.5	63(1)	17(1)	20(1)
$Nd_5Si_{1.2}Sb_{1.8}$[a]	62.5	15.0	22.5	63.9(4)	14.6(8)	22(1)
$La_5Ge_{1.32(6)}Sb_{1.68(4)}$	62.5	16.5	21.0	64.5(5)	14.2(5)	21.3(5)
$Ce_5Ge_{0.9}Sb_{2.1}$[a]	62.5	11.3	26.2	66.4(3)	10.8(5)	22.7(6)
$Pr_5Ge_{1.68(6)}Sb_{1.32(4)}$	62.5	21.0	16.5	64.7(4)	18.8(4)	16.4(1)
$Nd_5Ge_{1.14(6)}Sb_{1.86(4)}$	62.5	14.3	23.2	65(1)	15(1)	21(1)

[a] Occupancies of the *Tt* and Sb sites in these Rietveld refinements were fixed on the basis of the observed atomic compositions.

Among the binary antimonides RE_5Sb_3, the Mn_5Si_3-type structure is found for the majority of the trivalent *RE* elements.[8] The hydrogen-free β-Yb_5Sb_3-type structure has now been established with certainty for two trivalent *RE* members (Er and Tm), and the closely related Y_5Bi_3-type structure is found for *RE* = Er, Tm, and Lu.[9] Some of these binary antimonides (e.g., Y_5Sb_3, Er_5Sb_3) or the related ternary variants (e.g., $Gd_5Ni_xBi_{3-x}$) undergo complex temperature-dependent phase transitions among these structure types.[7,12,14] To test whether polymorphism might occur in the $RE_5Tt_xSb_{3-x}$ series, the thermal stability of two representative members, $Pr_5Si_xSb_{3-x}$ and $Pr_5Ge_xSb_{3-x}$, was examined at temperatures lower than their original formation at 800 °C. Annealing them at 600 °C or 400 °C for two-

 © 2009 Wiley-VCH Verlag GmbH & Co. KGaA, Weinheim

Table 2. Atomic coordinates and equivalent isotropic displacement parameters for $RE_5Tt_xSb_{3-x}$ (RE = La–Nd; Tt = Si, Ge).

Atom	Wyckoff position	Occupancy	x	y	z	U_{eq} or U_{iso} [Å^2][a]
$La_5Si_{1.40(2)}Sb_{1.60(2)}$						
La1	8*d*	1	0.06534(4)	0.04007(5)	0.19305(5)	0.0149(1)
La2	4*c*	1	0.00061(5)	1/4	0.53559(8)	0.0161(1)
La3	4*c*	1	0.21353(5)	1/4	0.84177(8)	0.0151(1)
La4	4*c*	1	0.29443(5)	1/4	0.36269(8)	0.0149(1)
Si1/Sb1	8*d*	0.20(1)/0.802(5)	0.32629(5)	0.00820(5)	0.07503(7)	0.0108(2)
Si2	4*c*	1	0.4849(3)	1/4	0.5712(4)	0.0180(7)
$Ce_5Si_{1.4}Sb_{1.6}$						
Ce1	8*d*	1	0.0640(3)	0.0396(5)	0.1948(5)	0.020(1)
Ce2	4*c*	1	–0.0025(7)	1/4	0.5287(8)	0.014(1)
Ce3	4*c*	1	0.2172(7)	1/4	0.8389(9)	0.022(2)
Ce4	4*c*	1	0.2952(6)	1/4	0.3620(8)	0.015(2)
Si1/Sb1	8*d*	0.2/0.8	0.3254(3)	0.0084(8)	0.0755(6)	0.007(1)
Si2	4*c*	1	0.484(2)	1/4	0.573(3)	0.007(1)
$Pr_5Si_{1.20(3)}Sb_{1.800(8)}$						
Pr1	8*d*	1	0.06469(3)	0.04151(4)	0.19032(4)	0.0125(1)
Pr2	4*c*	1	0.00116(4)	1/4	0.53725(6)	0.0135(1)
Pr3	4*c*	1	0.21478(4)	1/4	0.83970(6)	0.0132(1)
Pr4	4*c*	1	0.29435(4)	1/4	0.36394(6)	0.0124(1)
Si1/Sb1	8*d*	0.10(1)/0.900(4)	0.32648(4)	0.00953(4)	0.07477(6)	0.0106(1)
Si2	4*c*	1	0.4849(2)	1/4	0.5735(3)	0.0138(5)
$Nd_5Si_{1.2}Sb_{1.8}$						
Nd1	8*d*	1	0.0661(4)	0.0426(5)	0.1926(6)	0.018(1)
Nd2	4*c*	1	–0.0044(9)	1/4	0.5312(9)	0.018(2)
Nd3	4*c*	1	0.2192(6)	1/4	0.8391(9)	0.008(2)
Nd4	4*c*	1	0.2973(6)	1/4	0.3623(9)	0.013(2)
Si1/Sb1	8*d*	0.1/0.9	0.3265(4)	0.0099(8)	0.0756(7)	0.015(1)
Si2	4*c*	1	0.480(3)	1/4	0.590(4)	0.015(1)
$La_5Ge_{1.32(6)}Sb_{1.68(4)}$						
La1	8*d*	1	0.06507(3)	0.04199(4)	0.19496(4)	0.0151(1)
La2	4*c*	1	0.00102(4)	1/4	0.53162(6)	0.0154(1)
La3	4*c*	1	0.21526(4)	1/4	0.84016(6)	0.0146(1)
La4	4*c*	1	0.29368(4)	1/4	0.35956(6)	0.0144(1)
Ge1/Sb1	8*d*	0.15(3)/0.84(2)	0.32589(3)	0.00766(4)	0.07326(5)	0.0117(1)
Ge2	4*c*	1	0.48239(8)	1/4	0.5746(1)	0.0178(2)
$Ce_5Ge_{0.9}Sb_{2.1}$						
Ce1	8*d*	1	0.0640(4)	0.0430(5)	0.1978(6)	0.011(1)
Ce2	4*c*	1	0.0013(11)	1/4	0.5245(9)	0.010(2)
Ce3	4*c*	1	0.2197(7)	1/4	0.8357(9)	0.008(2)
Ce4	4*c*	1	0.2929(6)	1/4	0.3553(9)	0.006(2)
Sb1	8*d*	1	0.3270(4)	0.0041(9)	0.0766(7)	0.020(1)
Ge2/Sb2	4*c*	0.9/0.1	0.482(1)	1/4	0.582(2)	0.020(1)
$Pr_5Ge_{1.68(6)}Sb_{1.32(4)}$						
Pr1	8*d*	1	0.06634(3)	0.04351(4)	0.19371(4)	0.0133(1)
Pr2	4*c*	1	0.00144(4)	1/4	0.53281(6)	0.0152(1)
Pr3	4*c*	1	0.21752(4)	1/4	0.83488(6)	0.0139(1)
Pr4	4*c*	1	0.29306(4)	1/4	0.35475(6)	0.0142(1)
Ge1/Sb1	8*d*	0.34(3)/0.66(2)	0.32611(4)	0.00777(5)	0.06983(6)	0.0109(2)
Ge2	4*c*	1	0.48116(8)	1/4	0.5763(1)	0.0144(2)
$Nd_5Ge_{1.14(6)}Sb_{1.86(4)}$						
Nd1	8*d*	1	0.06502(2)	0.04345(3)	0.19011(4)	0.0120(1)
Nd2	4*c*	1	0.00178(3)	1/4	0.53498(5)	0.0119(1)
Nd3	4*c*	1	0.21689(3)	1/4	0.83644(5)	0.0126(1)
Nd4	4*c*	1	0.29386(3)	1/4	0.36039(5)	0.0118(1)
Ge1/Sb1	8*d*	0.07(3)/0.93(2)	0.32637(3)	0.00954(4)	0.07231(5)	0.0101(1)
Ge2	4*c*	1	0.48252(7)	1/4	0.5784(1)	0.0130(2)

[a] U_{iso} applies to $Ce_5Si_{1.4}Sb_{1.6}$, $Nd_5Si_{1.2}Sb_{1.8}$, and $Ce_5Ge_{0.9}Sb_{2.1}$, for which Rietveld refinements were performed. U_{eq} is defined as one-third of the trace of the orthogonalized U_{ij} tensor.

 © 2009 Wiley-VCH Verlag GmbH & Co. KGaA, Weinheim

week periods did not reveal any changes in the powder X-ray diffraction patterns. This observation suggests that either $RE_5Tt_xSb_{3-x}$ undergoes no phase transformation at lower temperature, or that they are quite stable kinetically.

Structure and Bonding

The crystal structures of eight members of the $RE_5Tt_xSb_{3-x}$ series have been determined by single-crystal or powder X-ray diffraction in the orthorhombic space group *Pnma* (Table 2; Figures S1 and S2). The structure type adopted, that of β-Yb_5Sb_3,[22] has a ternary ordered variant called the Ce_5RuGe_2-type where Ru occupies a 4*c* site and Ge an 8*d* site in place of the Sb atoms in the former.[23] Although analogous ternary germanides, antimonides, and bismuthides were initially assumed to be similarly ordered, it is now recognized that they can exhibit a significant homogeneity range arising from disorder within these sites.[7,14,24,25] In the transition-metal-containing antimonides $RE_5M_xSb_{3-x}$ (*RE* = Gd–Er, Y; *M* = Fe, Co, Ni, Cu), the value of *x* is always smaller than 1 because the mixing of *M* and Sb atoms occurs only in the 4*c* site, whereas the 8*d* site accommodates Sb atoms exclusively.[7,12–15] In contrast, in the new tetrel-containing antimonides $RE_5Tt_xSb_{3-x}$ (*RE* = La–Nd; *Tt* = Si, Ge), the value of *x* is normally *larger* than 1 because the situation is reversed, with the 4*c* site being occupied only by *Tt* atoms, whereas the 8*d* site accommodates a mixture of *Tt* atoms with the majority Sb atoms (Table 2).

A simple way to visualize the structure of $RE_5Tt_xSb_{3-x}$ is to assemble it from RE_6 trigonal prisms (Figure 3). These trigonal prisms share opposite triangular faces along the *b* direction to form infinite columns, which then fuse along edges to form a three-dimensional framework outlining large distorted hexagonal channels. The mixture of *Tt*/Sb atoms (8*d* site, labeled as *Tt*1/Sb1 but referred to simply as Sb1 for brevity in subsequent discussion) fills the centres of the RE_6 trigonal prisms, whereas *Tt* atoms (4*c* site, labeled as *Tt*2) are connected to *RE*1 atoms to form a ribbon of $[RE_2Tt_2]$ rhombs extending along the large hexagonal channels (Figure 4a). The distinctions noted between the $RE_5Tt_xSb_{3-x}$ (*RE* = La–Nd; *Tt* = Si, Ge; usually $x \geq 1$) and $RE_5M_xSb_{3-x}$ (*RE* = Gd–Er, Y; *M* = Fe, Co, Ni, Cu; $x \leq 1$) series indicate that size effects, perhaps in the form of radius ratio rules, may be one factor controlling the formation of this structure. Examination of the local coordination environments in $RE_5Tt_xSb_{3-x}$ (Figure 4b) clearly reveals that the 8*d* site (CN9, tricapped trigonal prismatic) will be preferred by the larger Sb atoms whereas the 4*c* site (CN7, capped distorted octahedral) accommodates only the smaller *Tt* atoms. The limiting radius ratios are 0.73 for a tricapped trigonal prismatic site and 0.59 for a capped octahedral site.[26] As confirmed by inspection of Table 3, the distances of surrounding *RE* atoms to the Sb1 site (3.2–3.6 Å) are generally longer than those to the *Tt*2 site (2.9–3.3 Å), consistent with the relative sizes of atoms (Pauling metallic radii R_1 of 1.17 Å for Si, 1.24 Å for Ge, and 1.39 Å for Sb).[27] If neutral atoms are assumed and Pauling metallic radii are chosen, the ratio r_{Sb}/r_{RE} always lies, no matter what the *RE* metal, in the range 0.82–0.88, which exceeds the critical value of 0.73 required to support the occupation of Sb atoms within the tricapped trigonal prismatic (8*d*) sites, consistent with the site preference observed in either the $RE_5Tt_xSb_{3-x}$ or $RE_5M_xSb_{3-x}$ series. Similarly, the ratios $r_{Si}/r_{RE} = 0.69–0.72$ for $RE_5Si_xSb_{3-x}$ (*RE* = La–Nd), $r_{Ge}/r_{RE} = 0.74–0.76$ for $RE_5Ge_xSb_{3-x}$ (*RE* = La–Nd), and $r_M/r_{RE} = 0.71–0.74$ for $RE_5M_xSb_{3-x}$ (*RE* = Gd–Er, Y) exceed the critical value of 0.59 required to fill the capped octahedral (4*c*) sites. It is tempting to suggest that the Ge atoms in $RE_5Ge_xSb_{3-x}$ can mix in the 8*d* sites because r_{Ge}/r_{RE} also exceeds 0.73, but then the same line of argument fails to explain the observed site preferences of Si atoms in $RE_5Si_xSb_{3-x}$ or *M* atoms in $RE_5M_xSb_{3-x}$. Nor does it account for the nonexistence, for example, of $RE_5Tt_xSb_{3-x}$ for the late *RE*, or $RE_5M_xSb_{3-x}$ for the early *RE* metals, since their radius ratios do not seem to preclude their formation. Lastly, despite their formation with the later or smaller *RE* elements, the corresponding distances in $RE_5M_xSb_{3-x}$ (*M* = Fe, Co, Ni, Cu) are surprisingly not much shorter [e.g., 3.1–3.5 Å (Sb–Y) and 2.9–3.1 Å (Ni/Sb–Y) in $Y_5Ni_{0.38}Sb_{2.62}$] than in $RE_5Tt_xSb_{3-x}$.[12]

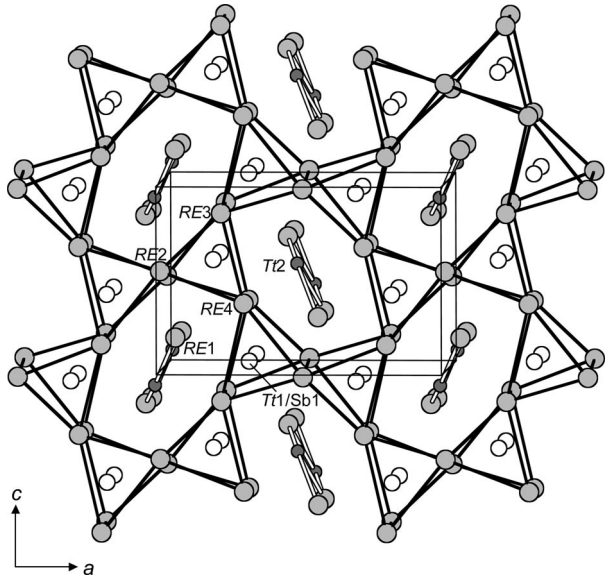

Figure 3. Structure of $RE_5Tt_xSb_{3-x}$ (*RE* = La–Nd; *Tt* = Si, Ge), emphasizing the connectivity of RE_6 trigonal prisms, viewed down the *b* direction. The large grey circles are *RE* atoms, the small solid circles are *Tt* atoms, and the medium open circles are Sb atoms.

One way to improve the arguments based on size effects is to include the role of electron transfer. Although the approximation of neutral atoms and metallic radii is certainly more realistic than that of fully charged species and ionic radii, it is clear that some degree of electron transfer must take place, but the directions will differ depending on the presence of a main-group vs. a transition metal. In $RE_5Tt_xSb_{3-x}$, the *RE* atoms will donate electrons to both *Tt* and Sb atoms, whereas in $RE_5M_xSb_{3-x}$, the *RE* and *M* atoms will donate electrons to the Sb atoms. That is, the *Tt*

 © 2009 Wiley-VCH Verlag GmbH & Co. KGaA, Weinheim

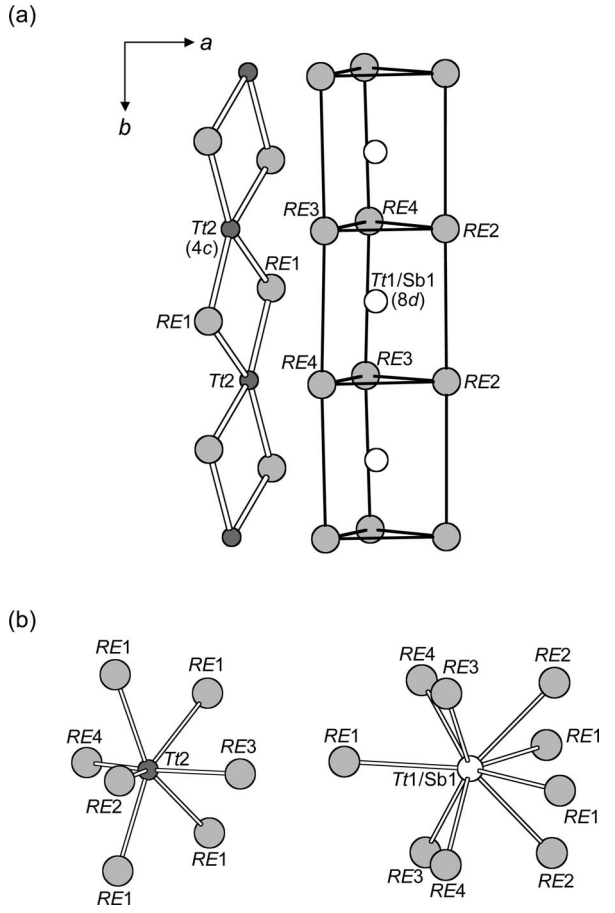

Figure 4. (a) One-dimensional ribbons of $[RE_2Tt_2]$ rhombs and columns of confacial RE_6 trigonal prisms extending along the *b* direction. (b) Local coordination environments around the *Tt*2 (4*c*) and *Tt*1/Sb1 (8*d*) sites.

atoms are likely anionic and have larger radii than the neutral species, whereas the *M* atoms are cationic and have smaller radii than the neutral species. In the discussion above, the key ambiguity can be traced to the fact that the r_{Tt}/r_{RE} or r_M/r_{RE} ratios are all quite close to 0.73, the critical value above which mixing of *Tt* atoms in the 8*d* site may take place. If r_{Tt} is replaced with larger and r_M with smaller values, then there should be an enhanced differentiation in the radius ratios, to the extent that r_{Tt}/r_{RE} may become >0.73 in $RE_5Tt_xSb_{3-x}$ and r_M/r_{RE} may become <0.73 in $RE_5M_xSb_{3-x}$. These corrections then account for the occurrence of mixing of *Tt* but not *M* atoms in the 8*d* site.

Interestingly, the lower bound for *x* was actually found to be slightly less than 1 in the investigation of the solid solubility in $La_5Ge_xSb_{3-x}$ ($0.9 \leq x \leq 1.6$). The Ge-poorest end-member for the solid solution in the cerium-containing series, $Ce_5Ge_{0.9}Sb_{2.1}$, showed the expected low Ge content (Table 1). In the crystal structure of $Ce_5Ge_{0.9}Sb_{2.1}$ (Table 2), the site occupation is now analogous to that in $RE_5M_xSb_{3-x}$ (*M* = Fe, Co, Ni, Cu), with 10% of the Ge atoms within the $[RE_2Ge_2]$ rhombs statistically substituted by Sb atoms.

Closer consideration of the electronic structure and bonding is helpful in determining what other factors besides size effects influence the structural stability in $RE_5Tt_xSb_{3-x}$ and $RE_5M_xSb_{3-x}$. Unlike the hydrogen-stabilized β-Yb_5Sb_3-type binary antimonides formed with divalent *RE* metals (e.g. Eu_5Sb_3H, Yb_5Sb_3H),[10,11] these ternary antimonides are not electron-precise. According to the Zintl-Klemm concept, electron counting for the idealized stoichiometric model "La_5GeSb_2" containing isolated Ge and Sb atoms implies the formulation $(La^{3+})_5(Ge^{4-})(Sb^{3-})_2(e^-)_5$, the five excess electrons remaining on the La atoms for use in

Table 3. Ranges of interatomic distances [Å] in $RE_5Tt_xSb_{3-x}$ (*RE* = La–Nd; *Tt* = Si, Ge).[a]

	$La_5Si_{1.40(2)}Sb_{1.60(2)}$	$Ce_5Si_{1.4}Sb_{1.6}$	$Pr_5Si_{1.20(3)}Sb_{1.800(8)}$	$Nd_5Si_{1.2}Sb_{1.8}$
*RE*1–*Tt*2	2.984(2)–3.127(3)	2.951(9)–3.11(2)	2.948(1)–3.069(2)	2.90(1)–3.18(3)
*RE*1–Sb1	3.462(1)–3.604(1)	3.423(4)–3.539(5)	3.394(1)–3.536(1)	3.354(6)–3.509(7)
*RE*1–*RE*2	3.564(1)	3.470(5)	3.528(1)	3.466(7)
*RE*2–*Tt*2	3.227(4)	3.27(2)	3.188(3)	3.08(3)
*RE*2–Sb1	3.292(1)–3.304(1)	3.236(9)–3.302(9)	3.245(1)–3.251(1)	3.168(9)–3.276(9)
*RE*3–*Tt*2	2.986(3)	3.01(3)	2.938(3)	3.00(3)
*RE*3–Sb1	3.316(1)–3.331(1)	3.270(6)–3.284(7)	3.263(1)–3.289(1)	3.224(8)–3.273(8)
*RE*4–*Tt*2	2.972(3)	2.92(3)	2.918(3)	2.91(3)
*RE*4–Sb1	3.328(1)–3.373(1)	3.280(6)–3.343(6)	3.284(1)–3.329(1)	3.242(7)–3.337(9)
Sb1–*RE*	3.292(1)–3.604(1)	3.236(9)–3.539(5)	3.245(1)–3.536(1)	3.168(9)–3.509(7)
*Tt*2–*RE*	2.972(3)–3.277(4)	2.92(3)–3.27(2)	2.918(3)–3.188(3)	2.90(3)–3.18(3)
	$La_5Ge_{1.32(6)}Sb_{1.68(4)}$	$Ce_5Ge_{0.9}Sb_{2.1}$	$Pr_5Ge_{1.68(6)}Sb_{1.32(4)}$	$Nd_5Ge_{1.14(6)}Sb_{1.86(4)}$
*RE*1–*Tt*2	2.990(1)–3.165(1)	2.980(5)–3.19(1)	2.946(1)–3.101(1)	2.942(1)–3.088(1)
*RE*1–Sb1	3.472(1)–3.609(1)	3.434(6)–3.517(6)	3.372(1)–3.550(1)	3.370(1)–3.532(1)
*RE*1–*RE*2	3.523(1)	3.417(7)	3.456(1)	3.497(1)
*RE*2–*Tt*2	3.292(2)	3.25(2)	3.193(2)	3.164(1)
*RE*2–Sb1	3.296(1)–3.308(1)	3.25(1)–3.29(1)	3.216(1)–3.230(1)	3.227(1)–3.232(1)
*RE*3–*Tt*2	3.034(2)	3.04(1)	3.004(2)	2.965(1)
*RE*3–Sb1	3.316(1)–3.341(1)	3.263(9)–3.335(9)	3.242(1)–3.267(1)	3.247(1)–3.284(1)
*RE*4–*Tt*2	2.988(1)	3.02(1)	2.940(2)	2.924(1)
*RE*4–Sb1	3.334(1)–3.378(1)	3.292(8)–3.364(8)	3.257(1)–3.310(1)	3.273(1)–3.321(1)
Sb1–*RE*	3.296(1)–3.609(1)	3.25(1)–3.517(6)	3.216(1)–3.550(1)	3.227(1)–3.532(1)
*Tt*2–*RE*	2.988(1)–3.292(2)	2.980(5)–3.25(2)	2.940(2)–3.193(2)	2.924(1)–3.164(1)

[a] The labels Sb1 and *Tt*2 refer to the majority component in these sites which may accommodate a mixture of both atoms.

 © 2009 Wiley-VCH Verlag GmbH & Co. KGaA, Weinheim

metal–metal bonding. The contribution of these homoatomic bonding interactions involving the *RE* atoms has been emphasized through previous band-structure calculations on both binary (Tm_5Sb_3, Y_5Sb_3) and ternary antimonides ($Y_5Ni_xSb_{3-x}$) with this structure type.[9,12] Calculations on a hypothetical model of $Y_5Ni_xSb_{3-x}$ in which Ni atoms are placed in the 8*d* site have suggested that doing so would destabilize the heteroatomic Y–Ni and Y–Sb interactions; structural relaxation to counteract these effects are also disfavoured by destabilizing the Y–Y interactions.[12]

To evaluate the site preferences in $RE_5Tt_xSb_{3-x}$, three ordered models of $La_5Ge_xSb_{3-x}$ were examined in which the Ge atoms occupy: (i) half of the 4*c* sites (x = 0.5 or $La_5Ge_{0.5}Sb_{2.5}$), (ii) all of the 4*c* sites (x = 1 or La_5GeSb_2), or (iii) all of the 4*c* and one-quarter of the 8*d* sites (x = 1.5 or $La_5Ge_{1.5}Sb_{1.5}$). The density of states (DOS) curves calculated for these models are similar (Figure 5). Although most of the La states are unoccupied and lie above the Fermi level, there are significant contributions below the Fermi level which mix with the Ge and Sb states, indicating that La–Ge and La–Sb bonding interactions will be important in stabilizing the structure. The crystal orbital Hamilton population (–COHP) curves for La–La, La–Ge, and La–Sb interactions for La_5GeSb_2 are shown in Figure 6. Homoatomic La–La bonding interactions are found primarily above the gap at –1 eV, whereas stronger heteroatomic La–Ge and La–Sb bonding interactions are found below. Increasing the degree of Ge substitution, from x = 0.5 to x = 1.5, reduces the number of electrons in the system, so that the Fermi level is shifted down closer to the gap near –1 eV (Figure 5). However, a rigid band approximation cannot be simply applied here to form conclusions about the change in bond strengths, because the relative contribution of Ge-based states below the Fermi level also becomes more important. The average integrated COHP values (–ICOHP), which are a measure of bond strength, for these interactions in the three models are listed in Table 4. The average –ICOHP values for La–La interactions differ slightly, but those for La–Ge and La–Sb change dramatically. Optimal bonding is observed in La_5GeSb_2 where the –ICOHP values are maximized. In contrast, the weakness of all contacts in hypothetical $La_5Ge_{0.5}Sb_{2.5}$ strongly disfavours its formation; for example, the La–Ge contacts are inherently much weaker (0.196 eV/bond). In $La_5Ge_{1.5}Sb_{1.5}$, both La–Ge and La–Sb bonding are also weakened relative to La_5GeSb_2, but not to the extreme extent as in $La_5Ge_{0.5}Sb_{2.5}$. Although this analysis shows that the composition can deviate from La_5GeSb_2, it is more favourable to do so towards the Ge-rich instead of the Ge-poor range, consistent with the observed solubility range of $0.9 \leq x \leq 1.6$ in $La_5Ge_xSb_{3-x}$.

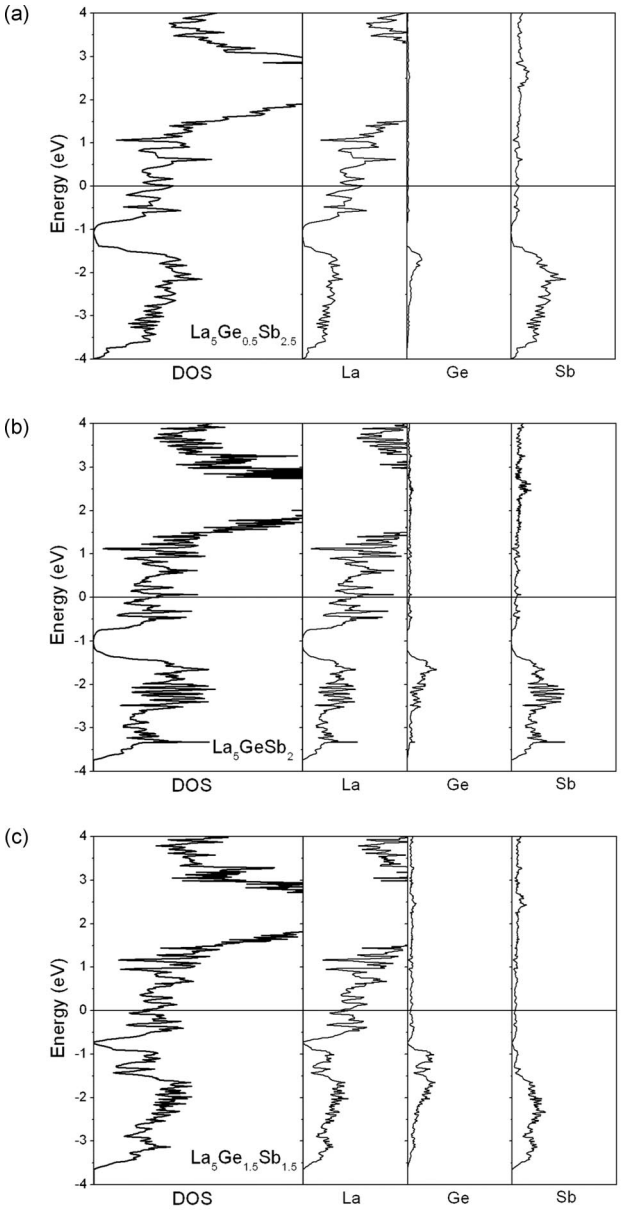

Figure 5. Density of states (DOS) and its La, Ge, and Sb projections for ordered models of (a) $La_5Ge_{0.5}Sb_{2.5}$, (b) La_5GeSb_2, and (c) $La_5Ge_{1.5}Sb_{1.5}$. The horizontal line at 0 eV marks the Fermi level.

Table 4. Average integrated crystal orbital Hamiltonian populations (–ICOHP) [eV bond^{-1}] in different models for $La_5Ge_xSb_{3-x}$.

Contact[a]	$La_5Ge_{0.5}Sb_{2.5}$	La_5GeSb_2	$La_5Ge_{1.5}Sb_{1.5}$
La–La	0.183	0.238	0.153
La–Ge	0.196	1.086	0.638
La–Sb	0.258	0.675	0.419

[a] For distances less than 4.2 Å.

Magnetic Properties

Magnetic measurements have been made for several representatives of the $RE_5Tt_xSb_{3-x}$ series, with the expectation that the only contributions to the magnetism will originate from f-electrons on the *RE* atoms. The La-containing compounds, $La_5Si_{1.2}Sb_{1.8}$ and $La_5Ge_{1.2}Sb_{1.8}$, exhibit temperature-independent paramagnetism with little dependence on the identity of the tetrel (χ_o = 0.001–0.002 emu/mol), consistent with trivalent La and the absence of localized unpaired electrons (Figure S3 in Supporting Information). The Ce-containing compounds could not be prepared in

 © 2009 Wiley-VCH Verlag GmbH & Co. KGaA, Weinheim

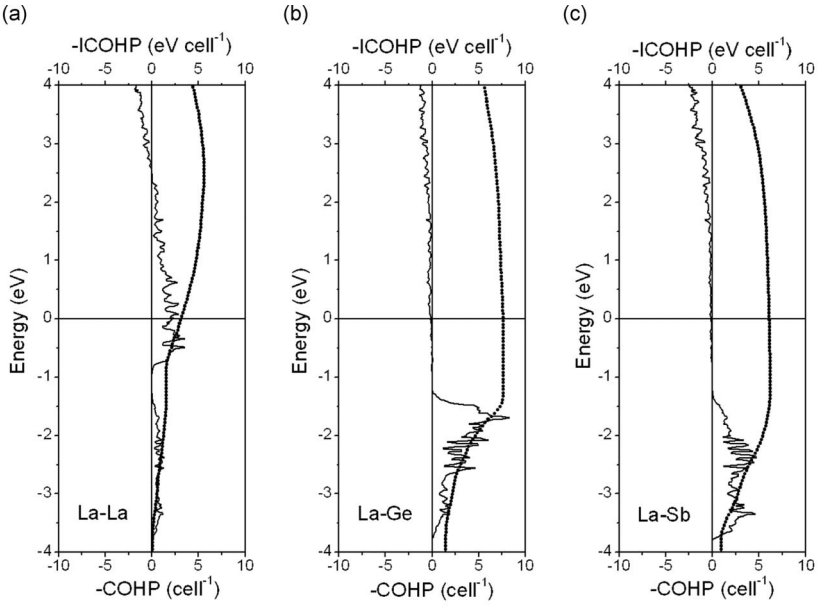

Figure 6. Crystal orbital Hamiltonian population (COHP) curves (solid line) and integrated COHP curves (dotted line) for (a) La–La, (b) La–Ge, and (c) La–Sb contacts in La_5GeSb_2. The horizontal line at 0 eV marks the Fermi level.

sufficiently pure form to permit measurements. For the Pr- and Nd-containing compounds, the zero-field-cooled dc magnetic susceptibilities (measured under an applied field of H = 5000 Oe), field-dependent magnetizations (measured at different temperatures), and ac susceptibilities indicate complex magnetic behaviour. Transition temperatures were located either from dc or ac magnetic susceptibility curves (Table 5).

Two members in the $Pr_5Ge_xSb_{3-x}$ series were measured to examine the effect of different Ge contents (x = 1.2 and 1.7). In $Pr_5Ge_{1.2}Sb_{1.8}$, the magnetic susceptibility curve shows two transitions at 4 K and ca. 30 K (Figure 7a). When the Ge content increases in $Pr_5Ge_{1.7}Sb_{1.3}$, the magnetic susceptibility is generally attenuated but the ca. 30 K transition becomes more prominent. The high-temperature paramagnetic regions of both curves are similar. The linear portions of the inverse magnetic susceptibility can be fit to the Curie–Weiss law, $\chi = C/(T - \theta_p)$. The effective magnetic moments (3.7 or 3.8 μ_B) derived from the Curie constant are slightly larger than the theoretical free-ion value for Pr^{3+} (3.6 μ_B), and the Weiss parameters θ_p are positive (32 or 21 K) for $Pr_5Ge_{1.2}Sb_{1.8}$ and $Pr_5Ge_{1.7}Sb_{1.3}$, respectively, indicating ferromagnetic coupling of the Pr^{3+} moments. Despite these similarities, the isothermal magnetization curves reveal different low-temperature magnetic structures: an approach to saturation for $Pr_5Ge_{1.2}Sb_{1.8}$ (Figure 7b) but metamagnetic behaviour for $Pr_5Ge_{1.7}Sb_{1.3}$ (Figure 7c) below ca. 30 K, and the appearance of hysteresis for both compounds below 4 K. The magnetic behaviour for $Pr_5Si_{1.2}Sb_{1.8}$ resembles that for $Pr_5Ge_{1.2}Sb_{1.8}$ except that the ca. 30 K transition is strongly suppressed (although it is still barely visible in the ac susceptibility curve), and the Weiss parameter has decreased from 32 K to 17 K (Figure 8a). The magnetization curves are also similar (Figure 8b).

The magnetic behaviour of $Nd_5Si_{1.2}Sb_{1.8}$ and $Nd_5Ge_{1.2}Sb_{1.8}$ is quite complex (Figure 8c–f). There are now at least three transitions, some ill-defined, seen in the magnetic susceptibility curves. Fitting of the inverse magnetic susceptibility in the paramagnetic regions yields similar effective magnetic moments (3.7 μ_B) and Weiss parameters (58–59 K) for both compounds. On the other hand, the magnetization curves show several step-like features at low temperatures, indicative of multiple metamagnetic states as a function of applied field.

Comparison to the parent binaries (RE_5Si_3, RE_5Ge_3, or RE_5Sb_3) provides little guidance because they adopt different structure types from $RE_5Tt_xSb_{3-x}$. For example, the Mn_5Si_3-type phases RE_5Ge_3[28–31] and RE_5Sb_3 (RE = Pr, Nd)[32] order antiferromagnetically, whereas the Cr_5B_3-type phases RE_5Si_3 (RE = Pr, Nd) order ferromag-

Table 5. Summary of magnetic data for $RE_5Tt_xSb_{3-x}$ (RE = Pr, Nd; Tt = Si, Ge).

	$Pr_5Si_{1.2}Sb_{1.8}$	$Pr_5Ge_{1.2}Sb_{1.8}$	$Pr_5Ge_{1.7}Sb_{1.3}$	$Nd_5Si_{1.2}Sb_{1.8}$	$Nd_5Ge_{1.2}Sb_{1.8}$
T_C [K] from:					
χ_{dc} curve	9, 30	4, 31	4, 30	10, 20, 62	11, 22, 65
χ'_{ac} curve	16, 28	not measured	29	25, 40, 62	15, 27, 64
θ_p [K]	17.2(6)	32.2(2)	20.8(4)	58.0(7)	58.8(3)
$\mu_{eff,\ meas}$ [μ_B/RE]	3.56(1)	3.69(1)	3.81(1)	3.75(1)	3.69(1)
$\mu_{eff,\ theor}$ for RE^{3+} [μ_B]	3.58	3.58	3.58	3.62	3.62

 © 2009 Wiley-VCH Verlag GmbH & Co. KGaA, Weinheim

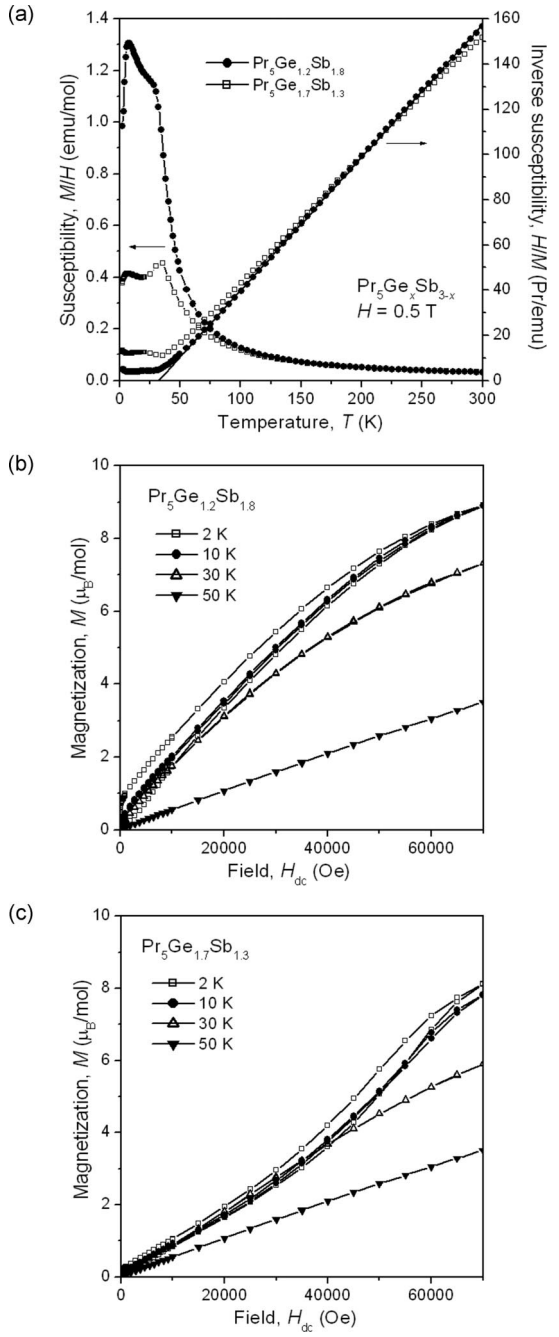

Figure 7. Magnetic data for $Pr_5Ge_xSb_{3-x}$ (x = 1.2, 1.7). (a) Magnetic susceptibility and its inverse, with a fit to the Curie–Weiss law indicated for $Pr_5Ge_{1.2}Sb_{1.7}$ by the solid line. (b) Isothermal magnetization at different temperatures for $Pr_5Ge_{1.2}Sb_{1.7}$. (c) Isothermal magnetization at different temperatures for $Pr_5Ge_{1.7}Sb_{1.3}$.

netically.[29,33,34] Magnetic measurements on related ternary antimonides with the β-Yb_5Sb_3-type structure are limited to those on Gd_5NiSb_2, where ferromagnetic ordering at 115 K was observed and the contribution of Ni atoms to the effective magnetic moment was considered to be negligible.[7] An important feature in these β-Yb_5Sb_3-type compounds is the presence of many close *RE*–*RE* contacts, as short as 3.4 Å in $RE_5Tt_xSb_{3-x}$ (Table 3), which gives rise to potentially strong magnetic interactions through direct coupling, in addition to indirect coupling via spin polarization of the conduction electrons.

Conclusions

The ternary antimonides $RE_5Tt_xSb_{3-x}$ illustrate the stabilization of the β-Yb_5Sb_3-type structure, previously found for only a few binary rare-earth antimonides RE_5Sb_3 and ternary transition-metal antimonides $RE_5M_xSb_{3-x}$, through partial substitution of Sb with Si or Ge. This substitution enables larger *RE* atoms (*RE* = La–Nd) to form this structure type. Because these ternary antimonides adopt a different structure from those of the parent binaries, they represent examples, still rare, of mixed-anion compounds exhibiting differential fractional site occupancy. Investigations are in progress to extend this work to ternary bismuthides.

Experimental Section

Synthesis: Initial reactions were performed in the course of investigating the La–Si–Sb and La–Ge–Sb phase diagrams. Starting materials were *RE* pieces (Hefa), Si lumps (Alfa-Aesar), Ge ingots (Alfa Inorganics, Ventron), and Sb ingots (Alfa-Aesar), each with 99.9% purity or better. Samples were prepared by arc-melting the elemental components in various ratios in a Centorr 5TA tri-arc furnace on a water-cooled copper hearth under argon in the presence of a Ti getter. The alloys were arc-melted twice and then sealed within evacuated fused-silica tubes. The samples were annealed at 800 °C for 20 d and then quenched in cold water. Phase identification was performed through powder X-ray diffraction on ground samples (with an Inel powder diffractometer equipped with a CPS 120 detector) and semiquantitative energy-dispersive X-ray (EDX) analysis on polished samples (with a Hitachi S-2700 scanning electron microscope). Single crystals of $La_5Si_xSb_{3-x}$ and $La_5Ge_xSb_{3-x}$ were found in the quenched alloys prepared from the molar ratio La/(Si or Ge)/Sb = 65:15:20. After the structures of these crystals were established from single-crystal X-ray diffraction studies, attempts were made to substitute other *RE* metals (*RE* = Ce–Nd, Sm, Gd) through similar arc-melting and annealing reactions with various loading compositions. These reactions were successful for *RE* = Ce–Nd, but not for *RE* = Sm and Gd, where only binary phases were obtained. For those reactions where single crystals could be obtained, elemental compositions were determined on polished samples through quantitative electron probe microanalysis (EPMA) measured with a JEOL 8900 microprobe analyzer (Table 1). The $La_5Ge_xSb_{3-x}$ series was selected for further investigation of the homogeneity range. Different samples in the range $0 \leq x \leq 3$ were prepared by arc-melting and annealing reactions. Phase analysis and evolution of cell parameters established the solid solubility range to be $0.9 \leq x \leq 1.6$ (Figure S1 and Table S1 in the Supporting Information).

Structure Determination: Suitable single crystals of $RE_5Si_xSb_{3-x}$ (*RE* = La, Pr) and $RE_5Ge_xSb_{3-x}$ (*RE* = La, Pr, Nd) were selected from reactions with various loading compositions for $RE_5Tt_xSb_{3-x}$. Single-crystal X-ray diffraction data were collected with a Bruker Platform/SMART 1000 CCD diffractometer at 22 °C by using ω scans. Structure solution and refinement were carried out with use of the SHELXTL (version 6.12) program package.[35] Face-indexed numerical absorption corrections were applied. For

 © 2009 Wiley-VCH Verlag GmbH & Co. KGaA, Weinheim

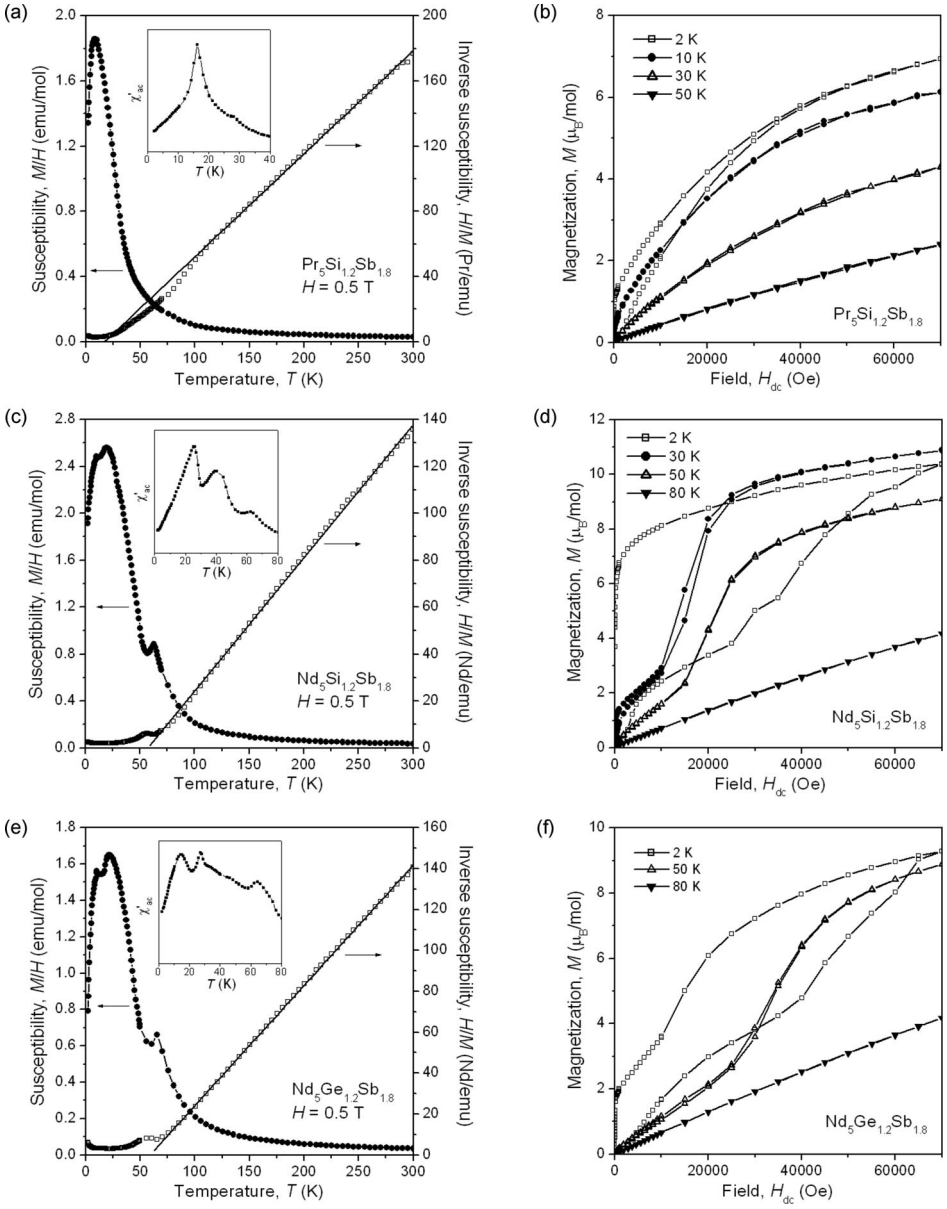

Figure 8. Magnetic data for (a)–(b) $Pr_5Si_{1.2}Sb_{1.8}$, (c)–(d) $Nd_5Si_{1.2}Sb_{1.8}$, and (e)–(f) $Nd_5Ge_{1.2}Sb_{1.8}$. The left panels show the zero-field-cooled dc magnetic susceptibility and its inverse as a function of temperature (with the insets highlighting low-temperature transitions in the ac magnetic susceptibility), and the right panels show isothermal magnetization curves at various temperatures.

all compounds, the centrosymmetric space group *Pnma* was chosen on the basis of intensity statistics. Initial atomic positions found by direct methods were consistent with the β-Yb_5Sb_3-type structure,[22] and refinements generally proceeded in a straightforward manner. Refinements on the occupancy factors confirmed that all *RE* sites are fully occupied. However, the distribution of *Tt* atoms in the two possible Sb sites (4*c* and 8*d*) had to be evaluated carefully. The refinement of $La_5Si_xSb_{3-x}$ is described here as an example. The idealized formula La_5SiSb_2 could be proposed initially on the basis of EDX analysis. Such a formula suggests that the 4*c* site is occupied exclusively by Si atoms and the 8*d* site by Sb atoms. Refinement of this ordered model, with the possibility of substoichiometry being permitted, led to partial occupancies of 0.94(1) Si in the 4*c* site and 0.850(3) Sb in the 8*d* site. Alternatively, substitutional disorder was invoked in which both sites were allowed to be occupied by a mixture of Si and Sb sites, subject to the restraint that the occupancies sum to 1.00(1) in each site. Refinement of this disordered model led to occupancies of 1.00(1) Si and 0.000(5) Sb in the 4*c* site, and 0.20(1) Si and 0.802(5) Sb in the 8*d* site. The third possible situation, in which both sites are substitutionally disordered and underoccupied, was not considered to be likely, given that related $RE_5M_xSb_{3-x}$ (*M* = Fe, Co, Ni, Cu) structures exhibit full occupancies in both sites and *M*/Sb disorder in only one site.[7,12–15] Guided in this manner, we have fixed the 4*c* site to be fully occupied exclusively by Si atoms and restrained the 8*d* site to be fully occupied by a mixture of Si and Sb atoms in the final refinement. The diffraction data for the other isostructural compounds were treated in a similar way, leading to refined formulas that agreed well with the EPMA results (Table 1), which are more precise than the EDX results. The possibility that interstitial impurities such as hydrogen atoms might be present was discounted on the basis that the parent binary trivalent rare-earth antimonides

 © 2009 Wiley-VCH Verlag GmbH & Co. KGaA, Weinheim

with the β-Yb_5Sb_3-type structure have been shown to be definitively hydrogen-free.[9] Because suitable single crystals of $RE_5Si_xSb_{3-x}$ (RE = Ce, Nd) and $Ce_5Ge_xSb_{3-x}$ were unavailable, their structures were refined from powder X-ray diffraction data, collected with an Inel powder diffractometer over 5 h. Initial positions were taken from the single-crystal structures determined above, and the full-profile Rietveld method was applied with use of the program LHPM-Rietica.[36] Because site occupancies are normally difficult to treat in the Rietveld method, they were not refined but rather fixed on the basis of the EPMA results (Table 1), with the assumption as before that the 4*c* site is fully occupied by *Tt* atoms and the 8*d* site by a mixture of *Tt* and Sb atoms. Both sites were constrained to have equal isotropic displacement parameters. The least-squares refinement included scale factor, background, zero point, cell parameters, occupancies, atomic coordinates, and isotropic displacement parameters. Fits of the Rietveld refinement results to the powder diffraction patterns are available in Figure S2 in the Supporting Information. For $Ce_5Ge_xSb_{3-x}$, the sample chosen was at the lower bound of the solid solution range (x = 0.9), which is below that for the idealized formula Ce_5GeSb_2 (x = 1.0). In this instance, the disorder of Ge and Sb atoms must be invoked in the 4*c* site and not in the 8*d* site, analogous to the case in $RE_5M_xSb_{3-x}$ (M = Fe, Co, Ni, Cu). Atomic positions were standardized with the program STRUCTURE TIDY.[37] Crystal data and further details of the data collections are given in Table 6. Final values of the positional and displacement parameters are given in Table 2. A detailed listing of interatomic distances is available in Table S2 (Supporting Information), and an abridged version is given in Table 3. Further data, in CIF format, have been sent to Fachinformationszentrum Karlsruhe, Abt. PROKA, 76344 Eggenstein-Leopoldshafen, Germany, as supplementary material No. CSD-420689 to -420693 and can be obtained by contacting FIZ (quoting the article details and the corresponding CSD numbers).

Band Structure: Tight-binding linear muffin tin orbital (TB-LMTO) band structure calculations were performed within the local density and atomic spheres approximations by using the Stuttgart TB-LMTO program.[38] To understand the bonding and solu-

Table 6. Crystallographic data for $RE_5Tt_xSb_{3-x}$ (RE = La–Nd; Tt = Si, Ge).

$RE_5Si_xSb_{3-x}$				
Empirical formula	$La_5Si_{1.40(2)}Sb_{1.60(2)}$	$Ce_5Si_{1.4}Sb_{1.6}$	$Pr_5Si_{1.20(3)}Sb_{1.800(8)}$	$Nd_5Si_{1.2}Sb_{1.8}$
Formula mass [amu]	928.68	934.73	957.41	974.06
Space group	*Pnma* (No. 62)	*Pnma* (No. 62)	*Pnma* (No. 62)	*Pnma* (No. 62)
a [Å]	12.6724(13)	12.5029(5)	12.401(2)	12.2970(6)
b [Å]	9.4205(10)	9.3597(4)	9.3328(16)	9.2798(5)
c [Å]	8.3191(9)	8.1872(3)	8.1740(14)	8.1208(4)
V [Å^3]	993.1(2)	958.09(7)	946.0(3)	926.68(8)
Z	4	4	4	4
$\rho_{calcd.}$ [g cm^{-3}]	6.211	6.477	6.722	6.979
Radiation	Mo-K_α, λ = 0.71073 Å	Cu-$K_{\alpha1}$, λ = 1.54056 Å	Mo-K_α, λ = 0.71073 Å	Cu-$K_{\alpha1}$, λ = 1.54056 Å
μ [mm^{-1}]	25.38	215.70	30.35	251.25
2θ range [°]	5.86–66.28	20.00–110.00	5.96–66.22	20.00–110.00
Refinement method	SHELXTL	Rietveld	SHELXTL	Rietveld
No. of data collected	11793	3103 data points	12383	3103 data points
No. of unique data	1970 (R_{int} = 0.097) [1426 with $F_o^2 > 2\sigma(F_o^2)$]	639 Bragg reflections	1875 (R_{int} = 0.083) [1498 with $F_o^2 > 2\sigma(F_o^2)$]	620 Bragg reflections
No. of variables	45	35	45	36
Residuals[a]	$R(F)$ [$F_o^2 > 2\sigma(F_o^2)$] = 0.039 $R_w(F_o^2)$ = 0.074	R_B = 0.015 R_p = 0.023 R_{wp} = 0.030	$R(F)$ [$F_o^2 > 2\sigma(F_o^2)$] = 0.032 $R_w(F_o^2)$ = 0.057	R_B = 0.011 R_p = 0.022 R_{wp} = 0.029
$RE_5Ge_xSb_{3-x}$				
Empirical formula	$La_5Ge_{1.32(6)}Sb_{1.68(4)}$	$Ce_5Ge_{0.9}Sb_{2.1}$	$Pr_5Ge_{1.68(6)}Sb_{1.32(4)}$	$Nd_5Ge_{1.14(6)}Sb_{1.86(4)}$
Formula mass [amu]	994.91	1021.61	987.21	1030.41
Space group	*Pnma* (No. 62)	*Pnma* (No. 62)	*Pnma* (No. 62)	*Pnma* (No. 62)
a [Å]	12.669(5)	12.5020(8)	12.337(6)	12.2982(11)
b [Å]	9.457(4)	9.4361(6)	9.283(4)	9.3222(9)
c [Å]	8.339(3)	8.2378(5)	8.144(4)	8.1599(8)
V [Å^3]	999.0(7)	971.8(1)	932.7(7)	935.5(2)
Z	4	4	4	4
$\rho_{calcd.}$ [g cm^{-3}]	6.615	6.979	7.030	7.316
Radiation	Mo-K_α, λ = 0.71073 Å	Cu-$K_{\alpha1}$, λ = 1.54056 Å	Mo-K_α, λ = 0.71073 Å	Mo-K_α, λ = 0.71073 Å
μ [mm^{-1}]	29.17	224.78	34.58	36.01
2θ range [°]	5.84–66.20	20.00–110.00	6.00–66.00	6.00–66.28
Refinement method	SHELXTL	Rietveld	SHELXTL	SHELXTL
No. of data collected	13100	3103 data points	12163	12244
No. of unique data	1988 (R_{int} = 0.074) [1582 with $F_o^2 > 2\sigma(F_o^2)$]	646 Bragg reflections	1847 (R_{int} = 0.088) [1405 with $F_o^2 > 2\sigma(F_o^2)$]	1868 (R_{int} = 0.063) [1531 with $F_o^2 > 2\sigma(F_o^2)$]
No. of variables	45	36	45	45
Residuals[a]	$R(F)$ [$F_o^2 > 2\sigma(F_o^2)$] = 0.033 $R_w(F_o^2)$ = 0.063	R_B = 0.017 R_p = 0.028 R_{wp} = 0.036	$R(F)$ [$F_o^2 > 2\sigma(F_o^2)$] = 0.032 $R_w(F_o^2)$ = 0.060	$R(F)$ [$F_o^2 > 2\sigma(F_o^2)$] = 0.027 $R_w(F_o^2)$ = 0.050

[a] $R(F) = \Sigma||F_o| - |F_c||/\Sigma|F_o|$; $R_w(F_o^2) = \{\Sigma[w(F_o^2 - F_c^2)^2]/\Sigma wF_o^4\}^{1/2}$; $w^{-1} = [\sigma^2(F_o^2) + (Ap)^2 + Bp]$ where $p = [\max(F_o^2,0) + 2F_c^2]/3$; $R_B = \Sigma|I_o - I_c|/\Sigma I_o$; $R_p = \Sigma|y_o - y_c|/\Sigma y_o$; $R_{wp} = \{\Sigma[w(y_o - y_c)^2]/\Sigma wy_o^2\}^{1/2}$.

 © 2009 Wiley-VCH Verlag GmbH & Co. KGaA, Weinheim

bility range in $La_5Ge_xSb_{3-x}$, three idealized ordered models at different levels of substitution x were examined: (i) $La_5Ge_{0.5}Sb_{2.5}$ (with Ge atoms in half of the 4*c* sites) was modeled in space group $P2_1/m$, (ii) La_5GeSb_2 (with Ge atoms in the 4*c* sites and Sb atoms in the 8*d* sites, i.e. the ordered Ce_5RuGe_2-type structure)[23] was retained in space group *Pnma*, and (iii) $La_5Ge_{1.5}Sb_{1.5}$ (with Ge atoms in the 4*c* sites and a quarter of the 8*d* sites) was modeled in space group $P\bar{1}$. The density of states (DOS) curves were calculated with use of a basis set consisting of La 6s/6p/5d/4f, Ge 4s/4p/4d, and Sb 5s/5p/5d/4f orbitals, with the La 6p, Ge 4d, and Sb 5d/4f orbitals being downfolded. Integrations in reciprocal space were carried out with an improved tetrahedron method over 36 irreducible *k* points for the model in *Pnma*. Inspection of the DOS curves revealed that the La 4f orbitals only contribute to conduction states, located well above the Fermi level, and do not participate in bonding interactions. For the purpose of determining crystal orbital Hamiltonian population (COHP) curves, these La 4f orbitals were additionally downfolded. (A representative DOS curve for La_5GeSb_2 with downfolded La 4f orbitals is shown in Figure S4 in the Supporting Information.)

Magnetic Measurements: Samples with a constant substitutional level, $RE_5Tt_{1.2}Sb_{1.8}$, were synthesized according to the procedure described earlier, and their purity was checked by powder X-ray diffraction. An additional sample, $Pr_5Ge_{1.7}Sb_{1.3}$, was prepared for comparison to $Pr_5Ge_{1.2}Sb_{1.8}$ to study the effect of different substitutional levels. Measurements of dc magnetic susceptibility were made on powders of all samples except for the Ce-containing ones (which contained a small amount of Ce_2Sb impurity) between 2 and 300 K with a Quantum Design 9T-PPMS dc magnetometer/ac susceptometer. All susceptibility values were corrected for contributions from the holder and underlying sample diamagnetism. Measurements of ac magnetic susceptibility were also made with a driving amplitude of 1 Oe and a frequency of 1000 Hz.

Supporting Information (see also the footnote on the first page of this article): Cell parameters for $La_5Ge_xSb_{3-x}$, full listing of interatomic distances, Rietveld refinement results, additional magnetic susceptibility plots, and density of states (for a calculation on La_5GeSb_2 with downfolded La 4f orbitals).

Acknowledgments

The Natural Sciences and Engineering Research Council of Canada and the University of Alberta supported this work. We thank Dr. Robert McDonald and Dr. Michael J. Ferguson (X-ray Crystallography Laboratory) for the X-ray data collection, Ms. Christina Barker (Department of Chemical and Materials Engineering) for assistance with the EDX analysis, and Dr. Sergei Matveev (Department of Earth and Atmospheric Sciences) for the electron probe microanalysis.

[1] K. A. Gschneidner Jr, V. K. Pecharsky, *Annu. Rev. Mater. Sci.* **2000**, *30*, 387–429.
[2] Y. Mozharivskyj, W. Choe, A. O. Pecharsky, G. J. Miller, *J. Am. Chem. Soc.* **2003**, *125*, 15183–15190.
[3] S. Misra, G. J. Miller, *J. Am. Chem. Soc.* **2008**, *130*, 13900–13911.
[4] V. K. Pecharsky, K. A. Gschneidner Jr, *J. Alloys Compd.* **1997**, *260*, 98–106.
[5] L.-M. Wu, S.-H. Kim, D.-K. Seo, *J. Am. Chem. Soc.* **2005**, *127*, 15682–15683.
[6] A. S. Chernyshov, Ya. S. Mudryk, V. K. Pecharsky, K. A. Gschneidner Jr, *J. Appl. Phys.* **2006**, *99*, 08Q102-1–08Q102-3.
[7] V. Svitlyk, F. Fei, Y. Mozharivskyj, *J. Solid State Chem.* **2008**, *181*, 1080–1086.
[8] O. L. Sologub, P. S. Salamakha, in *Handbook on the Physics and Chemistry of Rare Earths*, vol. 33 (Eds: K. A. Gschneidner Jr, J.-C. G. Bünzli, V. K. Pecharsky), Elsevier, Amsterdam, **2003**, pp. 35–146.
[9] S. Gupta, E. A. León-Escamilla, F. Wang, G. J. Miller, J. D. Corbett, *Inorg. Chem.* **2009**, *48*, 4362–4371.
[10] E. A. Leon-Escamilla, J. D. Corbett, *J. Alloys Compd.* **1998**, *265*, 104–114.
[11] E. A. Leon-Escamilla, J. D. Corbett, *Chem. Mater.* **2006**, *18*, 4782–4792.
[12] Y. Mozharivskyj, H. F. Franzen, *J. Alloys Compd.* **2001**, *319*, 100–107.
[13] A. V. Morozkin, R. Nirmala, S. K. Malik, *J. Alloys Compd.* **2005**, *394*, L9–L11.
[14] M. Zelinska, O. Zhak, S. Oryshchyn, V. Babizhetskyy, J.-Y. Pivan, R. Guérin, *J. Alloys Compd.* **2007**, *437*, 133–139.
[15] Yu. Verbovytsky, K. Łątka, *J. Alloys Compd.* **2008**, *450*, 272–275.
[16] A. O. Stetskiv, V. V. Pavlyuk, O. I. Bodak, *Ukr. Khim. Zh. (Russ. Ed.)* **1999**, *65*, 87–89.
[17] A. V. Morozkin, *J. Alloys Compd.* **2003**, *358*, L6–L8.
[18] A. Yu. Kozlov, V. V. Pavlyuk, *J. Alloys Compd.* **2004**, *370*, 192–197.
[19] P. Villars (Ed.), *Pauling File Binaries Edition*, Version 1.0, ASM International, Materials Park, OH, USA, **2002**.
[20] H. Bie, S. H. D. Moore, D. G. Piercey, A. V. Tkachuk, O. Ya. Zelinska, A. Mar, *J. Solid State Chem.* **2007**, *180*, 2216–2224.
[21] H. Bie, A. Mar, *Chem. Asian J.*, in press.
[22] G. D. Brunton, H. Steinfink, *Inorg. Chem.* **1971**, *10*, 2301–2303.
[23] R. E. Gladyshevskii, K. Cenzual, J. T. Zhao, E. Parthé, *Acta Crystallogr., Sect. C: Cryst. Struct. Commun.* **1992**, *48*, 221–225.
[24] O. L. Sologub, P. S. Salamakha, C. Godart, *J. Alloys Compd.* **2000**, *307*, 31–39.
[25] O. L. Sologub, P. S. Salamakha, E. Alleno, C. Godart, *J. Magn. Magn. Mater.* **2001**, *226–230*, 170–172.
[26] A. F. Holleman, E. Wiberg, *Inorganic Chemistry*, Academic Press, San Diego, **2001**.
[27] L. Pauling, *The Nature of the Chemical Bond*, 3rd ed., Cornell University Press, Ithaca, NY, USA, **1960**.
[28] K. H. J. Buschow, J. F. Fast, *Phys. Status Solidi* **1967**, *21*, 593–600.
[29] K. S. V. L. Narasimhan, H. Steinfink, E. V. Ganapathy, *J. Appl. Phys.* **1969**, *40*, 51–54.
[30] P. Schobinger-Papamantellos, K. H. J. Buschow, *J. Magn. Magn. Mater.* **1985**, *49*, 349–356.
[31] D. A. Joshi, A. Thamizhavel, S. K. Dhar, *Phys. Rev. B* **2009**, *79*, 014425-1–014425-7.
[32] J. K. Yakinthos, I. P. Semitelou, *J. Magn. Magn. Mater.* **1983**, *36*, 136–140.
[33] P. Boulet, F. Weitzer, K. Hiebl, H. Noël, *J. Alloys Compd.* **2001**, *315*, 75–81.
[34] N. Pinguet, F. Weitzer, K. Hiebl, J. C. Schuster, H. Noël, *J. Alloys Compd.* **2003**, *348*, 1–11.
[35] G. M. Sheldrick, *SHELXTL*, Version 6.12, Bruker AXS Inc., Madison, WI, USA, **2001**.
[36] B. Hunter, *LHPM-Rietica*, Version 1.7.7, International Union of Crystallography Commission on Powder Diffraction Newsletter, no. 20 (summer), **1998** (www.rietica.org).
[37] L. M. Gelato, E. Parthé, *J. Appl. Crystallogr.* **1987**, *20*, 139–143.
[38] R. Tank, O. Jepsen, A. Burkhardt, O. K. Andersen, *TB-LMTO-ASA Program*, Version 4.7, Max Planck Institut für Festkörperforschung, Stuttgart, Germany, **1998**.

Received: April 13, 2009
Published Online: July 2, 2009

 © 2009 Wiley-VCH Verlag GmbH & Co. KGaA, Weinheim